A Study of the E158 Spectrometer and Backgrounds

R. Boyce, E. Chudakov, R. Michaels, R. Holmes, K.S. Kumar, G.G. Petratos, P.A. Souder

March, 1999

1 Overview

The purpose of this document is to describe the spectrometer design in detail and estimate the background that one might expect under running conditions. Over the last year, detailed Monte Carlo calculations have been carried out in order to define and optimize collimators, verify the signal and background rates and estimate deposited power at various points in End Station A (ESA). We will focus on the three most important sources of backgrounds: photons, electrons and pions. We first briefly list the origin of these backgrounds:

- Sources of photon background are
  - Prompt and secondary photons from interactions in the target
  - Synchrotron radiation from the primary beam bending in the spectrometer dipoles
- Sources of electron background are
  - elastic electron proton scattering and its radiative tail
  - inelastic electron proton scattering and its radiative tail
- sources of pion background are
  - real and virtual photoproduction
  - deep inelastic electron proton scattering

We begin with a description of the layout in ESA, focusing on new developments since the proposal. We then discuss specific backgrounds and elaborate on design issues that are relevant in suppressing these sources of background. Finally, we summarize our results and discuss a schedule for assembling and commissioning the spectrometer and verifying the backgrounds.

2 ESA Design Considerations

The spectrometer consists of three dipole magnets in a "chicane" D$\bar{\text{D}}$D configuration followed by four quadrupole magnets. An engineering drawing of the layout of ESA is shown in Figure 1. The primary beam as well as the Møller electrons travel cleanly through all seven magnetic elements. The Møller electrons share the beam pipe with the primary beam for 55 meters downstream of the target. A flange separates the beamline vacuum from the shower counters that measure the Møller flux. This is shown in Fig. 2, which details the arrangement of detectors at the end of the beam pipe. Thus, any sources of secondary radiation from the intense, degraded primary beam into the Møller calorimeter is minimized.

The Møller shower counter is a total absorption calorimeter whose active medium is a pure Cherenkov radiator. The calorimeter will be between 15 to 25 radiation lengths (active and passive material interleaved), optimized to maximize the signal to background ratio. We therefore expect the background contamination from muons and neutrons to be negligible. In this report, no attempt is made to estimate the amount of muon or neutron background.

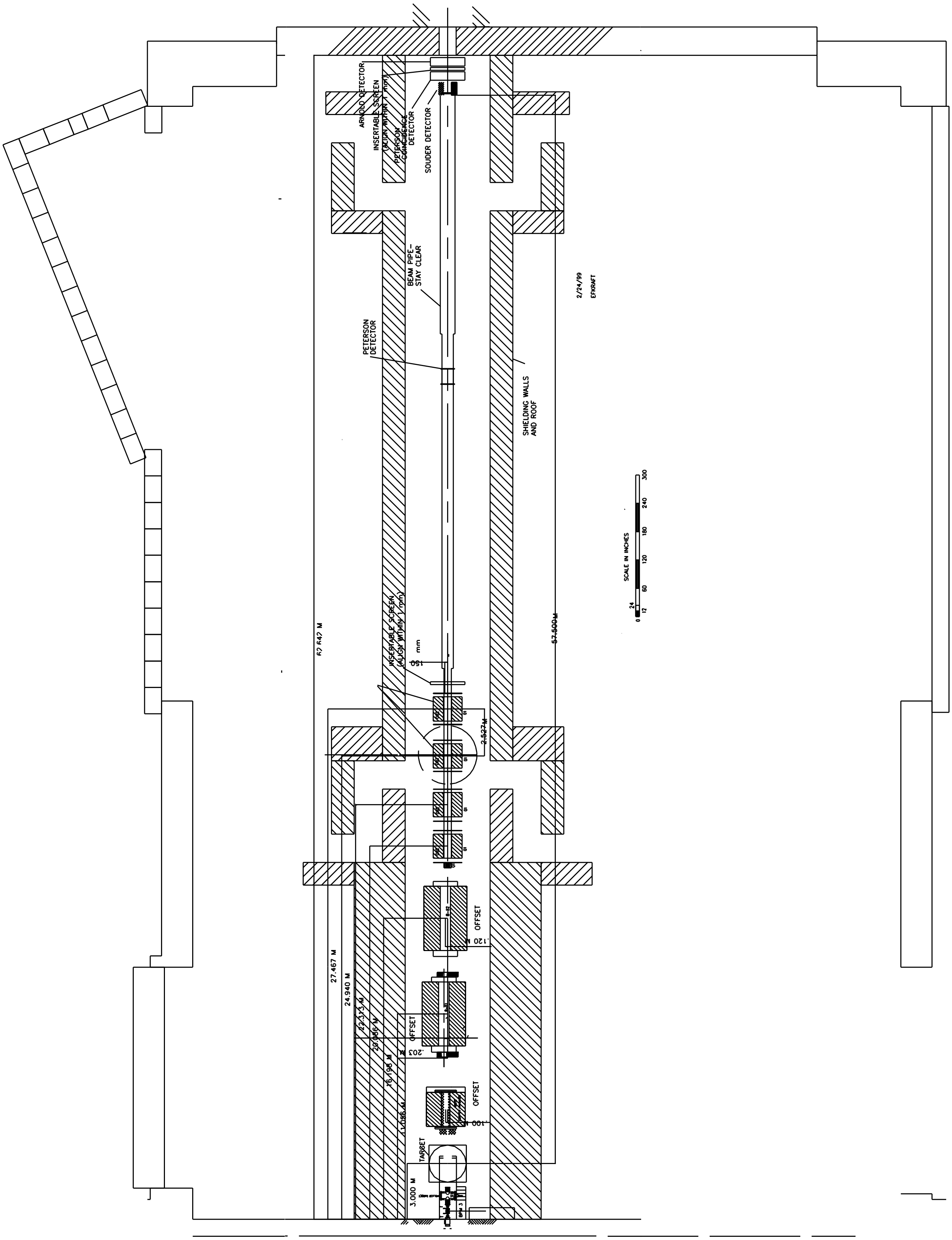

Figure 1: A drawing of the proposed E158 configuration of ESA is shown. The target chamber, magnetic elements and the long beam pipe leading to detectors at the ESA back wall are apparent. Proposed concrete shielding walls are also shown.

2.1 GEANT simulation

The full E158 spectrometer was simulated with a GEANT-based Monte Carlo. Included were the target (LH2 only), magnets, collimators, and beam pipe. The magnets included approximate representations of the iron yokes. The beam pipe was included from the downstream end of the fourth (and last) quadrupole to the detector plane. The incoming beam energy was 48.3 GeV. Simulations included all GEANT electromagnetic interactions except delta ray production; for some runs, synchrotron radiation was turned off.

Møller and Mott scattering generators, a pion photoproduction generator and the deep inelastic scattering generator LEPTO were included. There were two primary modes for optimizing the geometry: "Møller" or "beam-through". In the "Møller" mode each event begins with a Møller interaction in the target in a range of scattering angles (for the lower energy scattered electron) from 90° to 130°. This mode was used to determine appropriate collimation and to obtain the Møller spectrum in the detector.

In the "beam-through" mode each event begins with an electron entering the target; in most such events the only significant interaction in the target is bremsstrahlung. This mode was used in determining apertures for collimation, to check energy deposition in the magnets and collimators, and to obtain the photon spectrum in the detector. Figure 3 shows the GEANT geometry with typical beam-through events which originate at the target and weave their way through the seven magnetic elements.

In the following, the term "+bend" (to the right in Fig. 1) refers to the direction in which the first dipole would bend positive particles; "-bend" is the direction in which the first dipole would bend negative particles.

3 Photon Backgrounds

The main purpose of the chicane is to put the detector out of the line-of-sight of the target and to create a "two bounce system" for most of the photons with the help of strategically placed collimators: photons originating from radiative processes in the target can reach the detector only after bouncing twice on the vacuum pipe apertures or collimators. These collimators will be made of a tungsten alloy and we have used the Monte Carlo to tune their dimensions.

3.1 Primary Collimators

There are four collimators, one each in front of the second and third dipoles called herein CD2 and CD3; one in front of the first quadrupole, called CQ1; and one in the drift space downstream of the fourth quadrupole called CDR. The three dipoles and the first three collimators are shown in Fig. 4.

The CD2 and CD3 collimators are slabs (perpendicular to the beam) with a circular central hole for the bremsstrahlung photons and a rectangular aperture on the -bend side for the primary beam and Møller electrons. The second collimator (CD3) has in addition, a tungsten liner inside the upstream portion of the central hole. The central hole in CD3 is the only source of "one-bounce" photons and the liner minimizes the impact of the secondary emission of photons. These two collimators are intended to block relatively large angle photons that could reach the detectors, as well as spray from low-energy electrons that hit the dipoles. A cross sectional view of the collimators showing the two apertures in each collimator is shown in the raytrace diagram in Fig. 5.

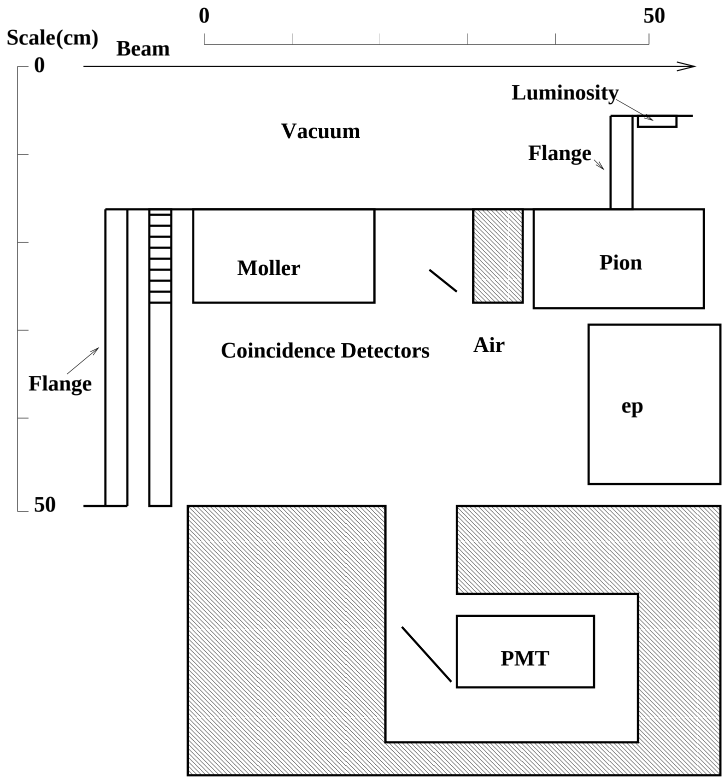

Figure 2: The proposed plan for the arrangement of detectors near the End Station wall is shown. The arrangement will be cylindrically symmetric about the beam axis.

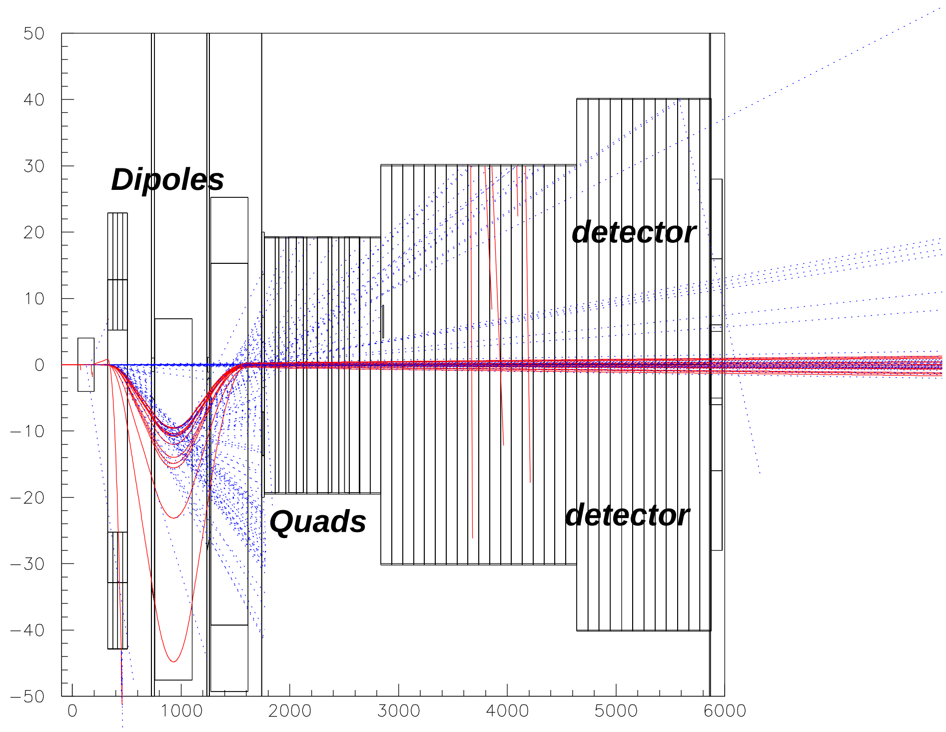

Figure 3: The GEANT geometry used in the simulation is shown with an example of several "beam-through" events. Solid lines are charged particles and dashed lines are neutral particles. Units are in cm.

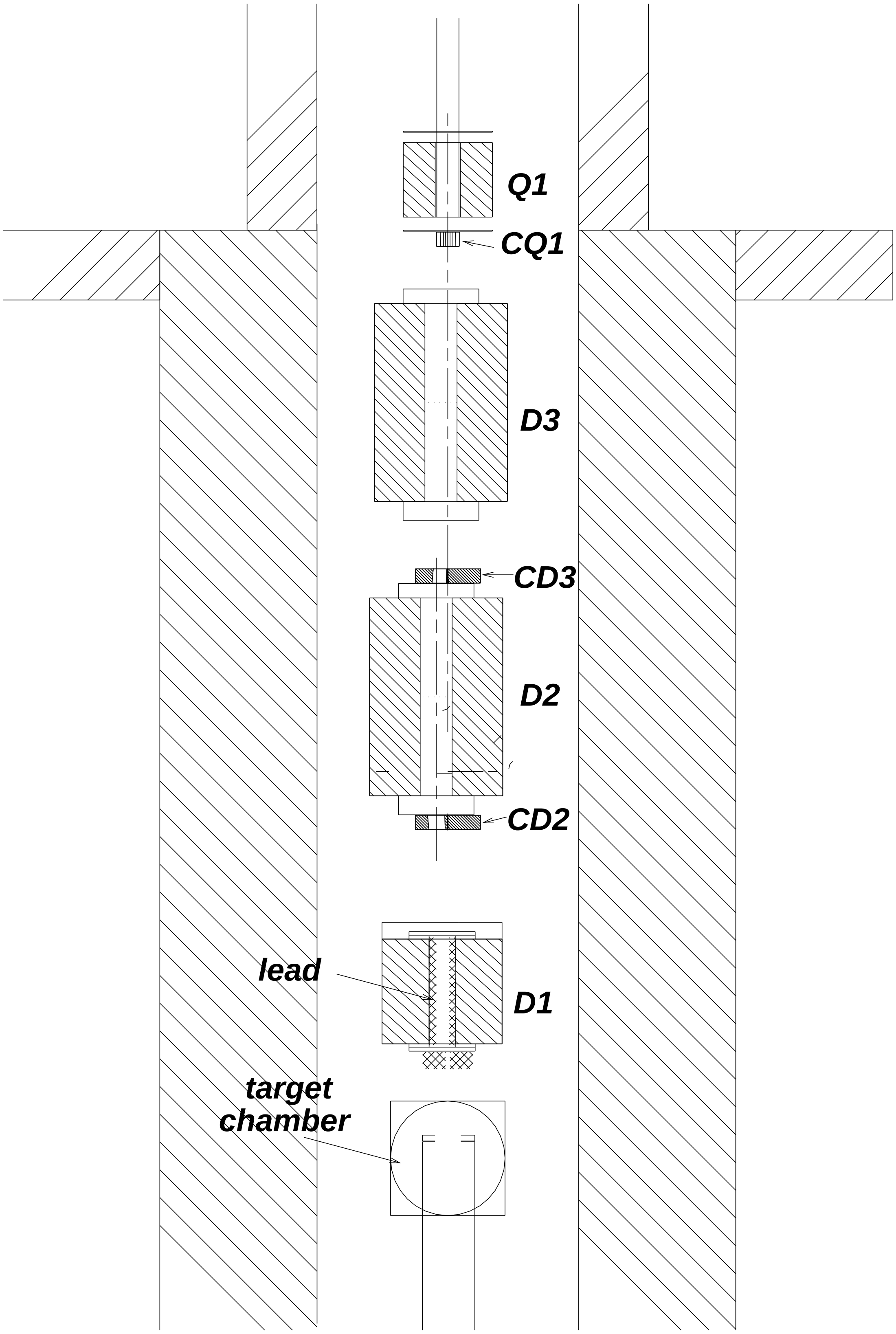

Figure 4: A closeup look at the first three dipoles and the first quadrupole and the first three collimators.

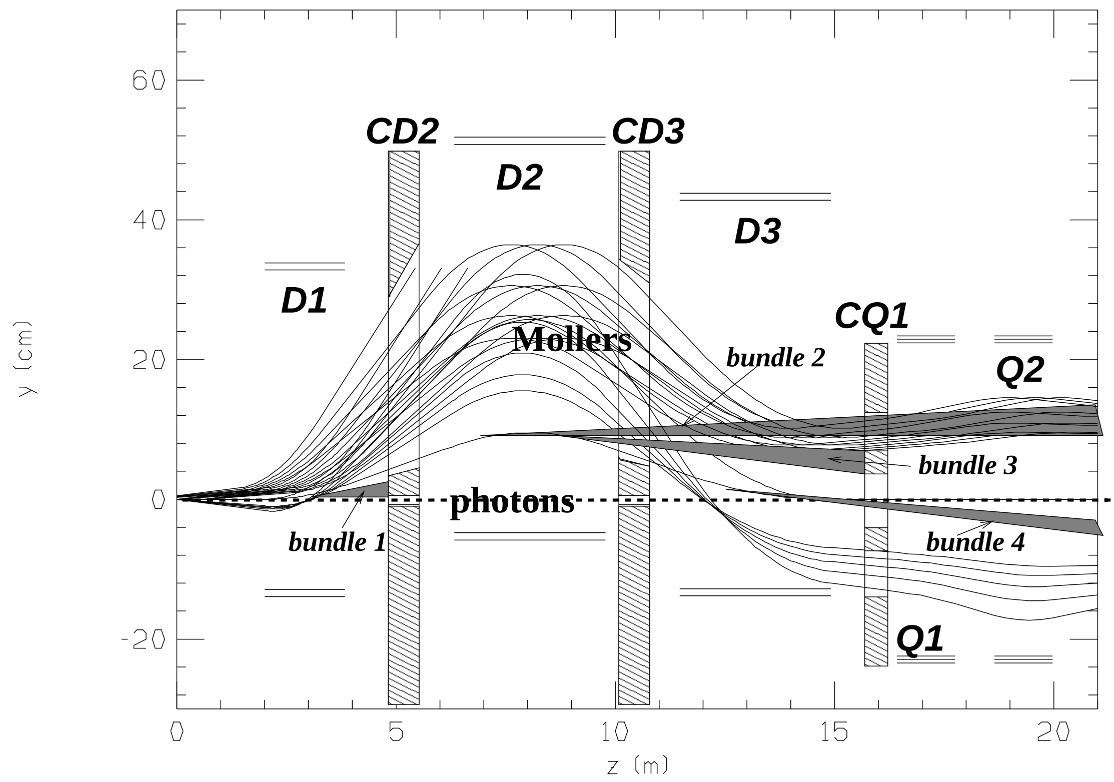

Figure 5: The position of the three main physics collimators are shown with respect to the dipoles and raytraces of Møller electrons and beam electrons. Also shown are the four bundles of synchrotron rays that point to the Møller detectors.

The CQ1 collimator consists of a lead slab with a circular hole inside of which is suspended a lead ring, thereby defining a circular central hole for the beam and photons and an annular aperture for the Møller electrons. It has a "spoke" between the two rings. This "spoke", and the CDR collimator, will be discussed later in the section on synchrotron radiation. The role of CQ1 (see Fig. 5) is to select electrons with the correct angles to be Møller electrons in the range of scattering angles $\theta = 90^\circ$ to 120° in the center of mass (corresponding to an energy range of 12.075–24.15 GeV for this beam energy).

3.2 Synchrotron Collimators

Because the main beam is being sent through a dipole chicane, a significant amount of synchrotron radiation is produced in the bend plane. Gammas averaging about 1 MeV per incident beam electron arrive at the Møller detector, along a 1 cm thick band in the horizontal plane. There are potentially four sets of trajectories (or "bundles") for synchrotron radiation into the Møller detector, as shown in Fig. 5:

1. Origin at first dipole, heading toward -bend side. These are collimated by the existing CD2 collimator.

2. Origin at second dipole, heading toward -bend side. These photons overlap the Møller electron trajectories nearly all the way from their origin to the detector. Collimating them requires giving up a little solid angle for Møllers. Since supporting and cooling the inner ring of CQ1 also requires sacrificing solid angle, a "spoke" was introduced to perform both functions.

3. Origin at second dipole, heading toward +bend side. These can be collimated by choosing a small enough inside diameter for the inner ring of CQ1 if they come from full-energy beam electrons. Radiative electrons can emit synchrotron radiation which can go through the Møller aperture of CQ1 and hit the detector. These photons are stopped by the same "spoke" that is used for bundle 2.

4. Origin at third dipole, heading toward +bend side. These photons are at smaller radii than the Møllers all the way from their origin to the detectors, which means they can be collimated easily, but only by installing a collimator that "hangs in midair" between the Møllers and the beam.

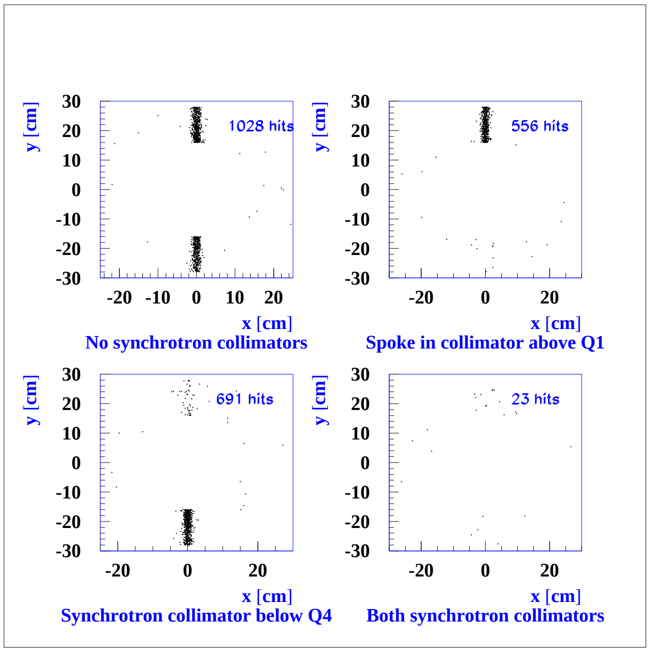

Figure 6: Position distribution (y vs. x) for synchrotron photons in the Møller detector from 2000 beam-through events. (Top left) No synchrotron collimation; (Top right) With "spoke" in CQ1; (Bottom left) With collimator CDR; (Bottom right) With CQ1 "spoke" and CDR.

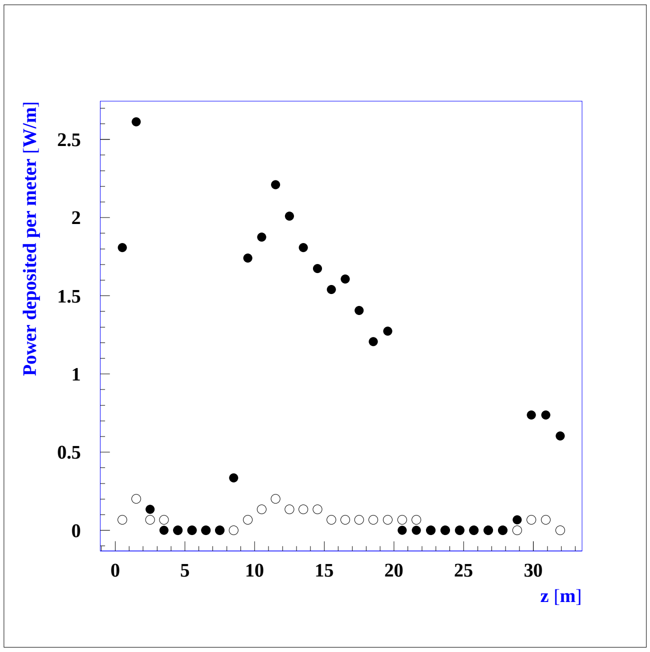

Figure 7: Energy deposition in Watts per meter of beam pipe as a function of distance (in m) from Q4, on the -bend side (open circles) and +bend side (filled circles).

The synchrotron radiation into the Møller detectors can be decreased about 2 orders of magnitude with the following collimators:

- A "spoke" between the inner and outer rings of the Q1 collimator, in the bend plane on the -bend side, 1.2 cm thick and 12 cm long. This collimator reduces the acceptance for Møllers by 2.2%.
- A slab 287.4 cm (center to center) downstream of Q4, in the bend plane on the +bend side, 2.0 cm thick, 12 cm long, and 5 cm wide. Its center is 6.5 cm from the nominal beam, so it covers radii from 4.0 cm to 9.0 cm from the beam. This slab would have to be supported, probably cutting into the Møller acceptance slightly.

Object	Deposition (Watts)	
	-bend	+bend
Dipole D1		
1st 25%	20	87
2nd 25%	60	281
3rd 25%	188	375
4th 25%	315	302
Collimators		
CD2	1005	
CD3	74	
CQ1 (inner ring)	54	
CQ1 (outer ring)	34	
CQ1 (spoke)	27	
CDR	13	
Beam pipe		
1st 2 meters	$<$ 0.2 per m	$<$ 2.6 per m
Next 18 meters	$<$ 0.2 per m	$<$ 2.2 per m
Last 12 meters	$<$ 0.1 per m	$<$ 0.8 per m

Table 1: Energy deposition in first dipole, collimators, and beam pipe.

Figure 6 shows the effects of the collimators on synchrotron radiation. With the "spoke" and the downstream slab absent, there are 1028 hits in 2000 events. This would correspond to a signal to noise of more that 1:1 at the Møller detectors (assuming 100% efficiency for absorbing a few MeV photon). Average photon energy is about 3 MeV, or about 1.5 MeV per event. With both the "spoke" and the new collimator there are only 23 hits, or about 0.03 MeV per event. This corresponds to a background of less than 3%. (This energy is less strongly peaked near the bend plane, so detector segments near the bend plane will see an even greater reduction in synchrotron energy.)

4 Energy Deposition

Energy deposition in the dipoles and collimators was studied using 20000 beam-through events. Results are summarized in Table 1. The pole faces of the first dipole are struck by low energy electrons (on the -bend side) and positrons (on the +bend side). There are fewer positrons at a given momentum but, due to the offset of D1 toward the -bend side, a larger fraction of the positrons hits the pole face and the average energy of the positrons that hit is higher.

We propose to line the dipole with 7.5 cm of lead which reduces energy deposition in the iron by more than a factor of 100. In this configuration, an average of 580 W is deposited in the lead lining the -bend pole of D1, and about 1 kW in the +bend pole. Most of this energy is deposited in the downstream end of the magnet. On the -bend side 54% of the energy is deposited in the most downstream 25% of the pole, while on the +bend side 92% of the energy is deposited in the last 75% of the pole. Hits are localized within about a centimeter of the bend plane.

Synchrotron radiation deposits up to about 3 W per meter of beam pipe, in the area from about

10 to 20 m downstream of Q4 on the +bend side. The energy deposition is shown Fig. 7 as a function of distance from the last quadrupole.

5 Electron Background

The purpose of the quadrupoles is to focus the Møller scattered electrons of interest in a concentrated detector area resulting in a minimal contamination from electrons from radiative scattering off target protons. Since we plan to integrate the scattered flux, it is important to simulate and verify the amount of background from other processes that might arrive at the same location as the Møller electrons in the vicinity of the detector.

5.1 Radiative Elastic Scattering off the Proton

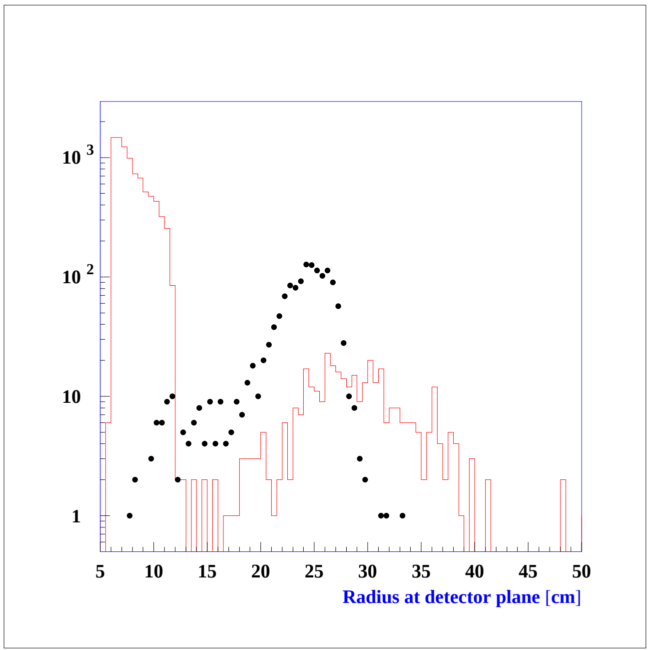

Figure 8: Distributions of Møller electrons (dots) and Mott electrons (histogram) are shown as a function of radial distance from the beam (in cm).

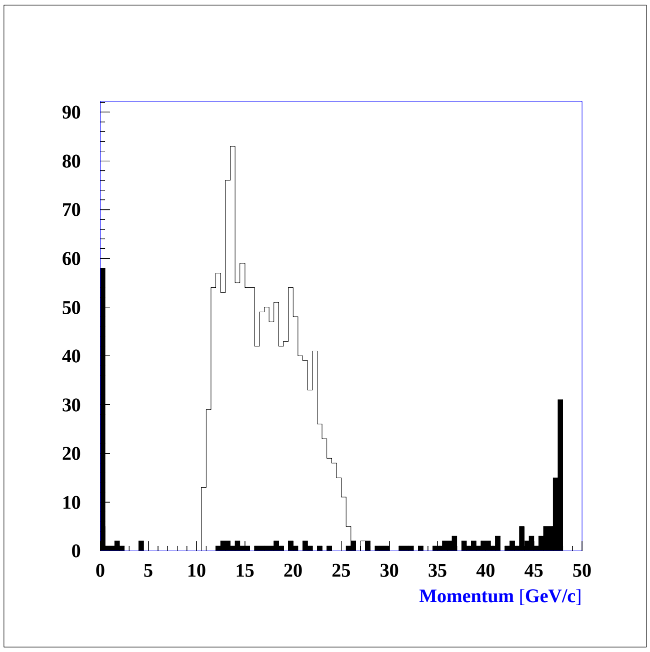

Figure 9: Distributions of Møller electrons and Mott electrons (filled histogram) are shown as a function of momentum (GeV) at the Møller detector $(18 < r < 28)$ (cm)

The most important background under the Møller peak is elastic e-p scattering and its radiative tail: about 15% of the Møller signal. All other sources of background are less than a percent each. In order to be able to account for this background with small systematic errors, we are taking the following steps:

- A detailed Monte Carlo simulation with attention to radiative corrections
- Auxilliary integrating detectors adjacent to the Møller detectors (where the flux is dominated by radiative e-p events) to measure the asymmetry of the e-p background

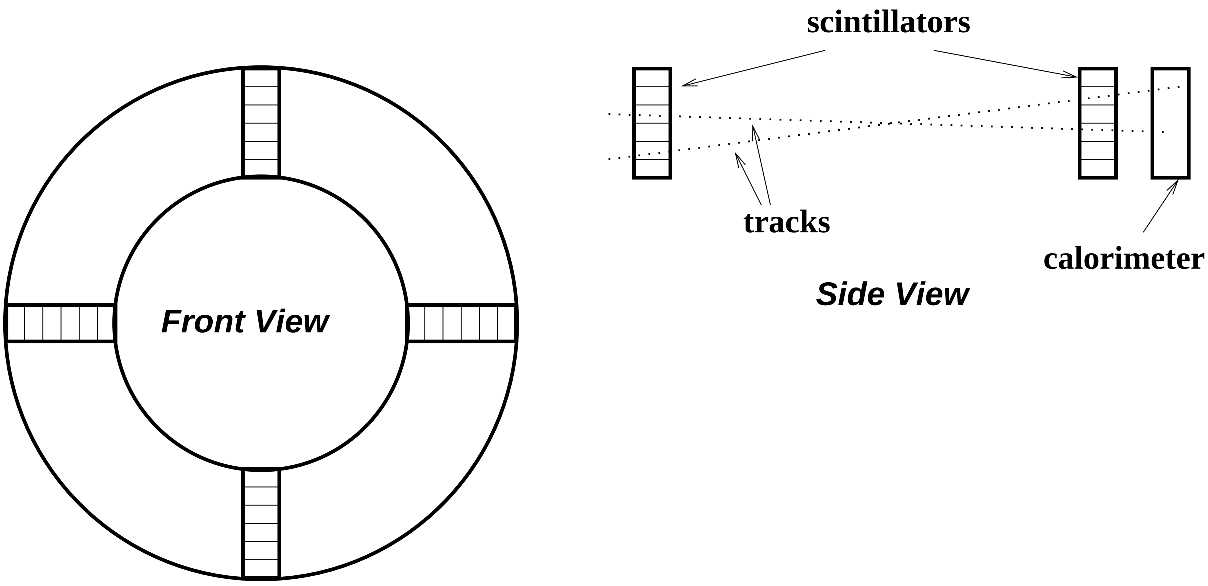

Figure 10: A conceptual design of the Møller counting detectors is shown.

- Coincidence detectors to be run at low rate in order to verify the Monte Carlo calculations.

We elaborate on the above mentioned issues below.

5.1.1 Simulation Results

We have incorporated a Mott scattering generator into our Monte Carlo which properly takes into account the degradation of the primary beam as it traverses the thick hydrogen target. Mott electrons were generated in the range 1 mrad $< \theta_{\rm lab} <$ 10 mrad. The results are shown in Figs. 8 and 9, where the distribution of Møller and Mott electrons from the hydrogen target are shown as a function of radial distance from the beam (Fig. 8) and as a function of momentum for those electrons that enter the Møller detector (Fig. 9).

5.1.2 Integrating Mott Detector

As seen in Fig. 8, the Mott electrons overlap the Møller peak at the detector but extend out to larger radii, beyond the edge of the Møller peak. We propose to measure the electroweak asymmetry at these larger radii with auxilliary detectors similar in design to the Møller detector (see Fig. 2). This asymmetry would serve as a crosscheck of the e-p effective weak neutral current coupling constant at low Q^2. The resulting asymmetry will be used to correct the the Møller asymmetry to account for the Mott background under the Møller peak.

5.1.3 Coincidence Detectors

In order to calculate the asymmetry of the Mott background under the Møller peak, the asymmetry from the Mott detector will be used with an additional correction for the different Q^2 ranges of the Mott electrons in the two different regions. The range of Q^2 will be calculated in a Monte Carlo, but we plan to verify the characteristics of the Møller and Mott electron kinematics with a separate system of detectors that will operate at low rates.

The goals of these detectors, that will use coincidence methods and full kinematic recontruction of individual tracks, are:

- verify the properties of the spectrometer by mapping out the position of the Møller stripe,
- measure the Mott and inelastic radiative tails and pion rates.

We propose to use scintillation counters with radial segmentation along four symmetric azimuthal slices in front of the Møller calorimeter and a second set of counters for measuring the angle of the tracks many meters upstream. Under the reasonable assumption that most tracks will have the same azimuthal angle, a coincidence between the two scintillator planes should establish the angle of the track. With additional information on energy deposition from the Møller calorimeter, it will then be possible to separate pions and Møtt electrons from Møller electrons.

A conceptual design of the scintillator detector is shown in Fig. 10. One important issue is to reduce the rates to a manageable level. We would like the rate to be 1 trigger per pulse in each 1 cm^2 counter. This requires that the rate be reduced by a factor of 10^5 from normal running conditions. We propose to do this by setting up the beam tune at 2×10^9 electrons per pulse, where there is no significant beam loading. We would then pulse a special Pockels cell to gain an additional factor of 1000 in extinction of the laser beam. The beam would still be pulsed at 2×10^9 at 1 Hz in order to tune and keep track of the beam.

5.2 Radiative Inelastic Scattering off the Proton

The radiative elastic e-p scattering process discussed above is dominated by electrons that radiate externally before elastic scattering. The same is true for inelastic scattering. Since we will have carefully verified the radiative e-p rate, it is sufficient to calculate the ratio of the various radiative processes to that of elastic scattering.

As detailed in Appendix C.3 (page 48) in the proposal, radiative inelastic events off the Δ is estimated to be 1.7% of the elastic e-p rate. Therefore, inelastic scattering off the Δ adds a dilution of 2.5×10^{-3} to the Møller asymmetry. The asymmetry of this background is likely to be five times larger than the Møller asymmetry (the unknown $\Delta - Z^0$ coupling), leading to a 1.2% correction to the Møller asymmetry.

For additional resonances and the continuum, as estimated in Appendix C.4 of the proposal, the dilution is estimated to be about 1%. The asymmetry correction, is estimated to be about 3%.

5.3 Inelastic Scattering of Primary Beam Electrons

One can calculate the total inelastic cross section in the approximation $\theta \ll 1$ and $Q^2 \ll \nu^2$. By integrating the inelastic double differential cross section (Appendix C.2 of the proposal) over the momentum and $\theta_{\rm lab}$ range of the Møller electrons, one obtains a cross section of 40 nBarn. This gives a dilution factor of the measured asymmetry of 2×10^{-3} and an asymmetry correction (due to the $\rho - Z^0$ coupling) of 2%.

6 Pions

There are two primary sources of pion background: photoproduction and deep inelastic scattering. High energy pions, unlike electrons, can punch through the collimators and it is important to investigate whether residual shower particles contaminate the Møller signal significantly. As described below, we have investigated both sources of pion background by careful Monte Carlo simulation of pions traversing the optimized spectrometer geometry.

6.1 Real and Virtual Photoproduction

As is estimated in Appendix C.6 in the proposal, we expect that pions from real photoproduction dilutes the asymmetry by at most 0.5%. Further, the asymmetry would be similar to that of elastic p-p scattering. This gives us the estimate for the asymmetry correction of 1.5%.

The dilution from pion virtual photoproduction is negligible: $< 2 \times 10^{-3}$. The asymmetry correction on the other hand is larger than that for real photoproduction and is estimated to be 1.3%.

6.1.1 Simulation Results

We have carried out a simulation of pion photoproduction into our optimized spectrometer geometry. Pions were generated in the range 1 mrad $< \theta_{\rm lab} <$ 120 mrad and in the momentum range from 5% to 95% of the beam energy using an emperical cross section derived from old SLAC data. The two dimensional distribution of momentum vs $\theta_{\rm lab}$ is shown in Fig. 11, along with the corresponding distribution for accepted Møller events. Figure 12 shows the momentum distribution of the fraction of pions that are observed at the Møller detector.

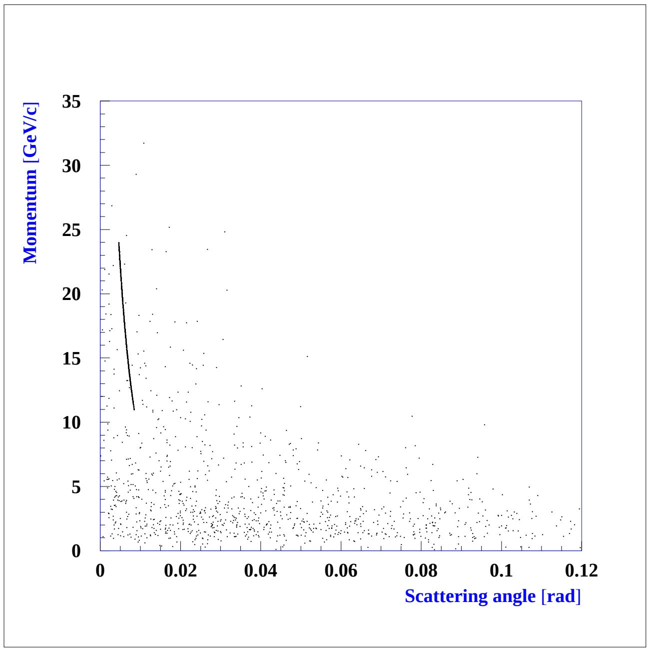

Figure 11: A scatter plot of the energy vs laboratory scattering angle of photoproduced pions by the Monte Carlo generator is shown, along with the accepted Møller electron stripe.

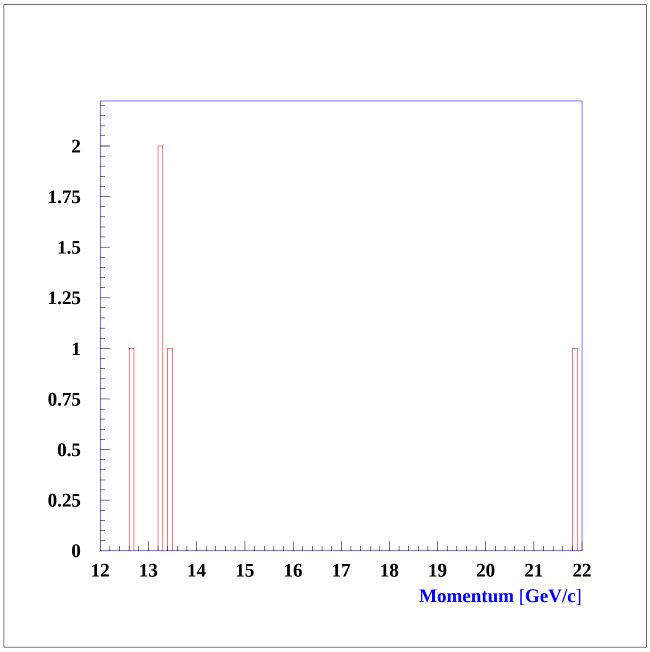

Figure 12: Momentum distribution of those pions that arrive at the Møller detector is shown, for a luminosity corresponding to 12000 detected Møller electrons

The result of the simulation is that the pions from photoproductoin produce a very small dilution 2×10^{-4}, an order of magnitude less than the estimate made in the previous section, which should be viewed as a conservative upper limit.

6.2 Deep Inelastic Scattering

Electrons from deep inelastic scattering are produced at much larger angles than the signal Møller electrons, but there is a possibility of background from the pions produced in the process. This background is potentially dangerous because the electroweak asymmetry is three orders of magnitude bigger than the Møller asymmetry. In Appendix C.5 of the proposal, it was estimated that the dilution factor from these pions is 2×10^{-4} and the asymmetry correction is 1%.

As we describe below, we are simulating this background with a detailed Monte Carlo as well as building an auxilliary pion detector in order to verify the size of the background asymmetry correction.

6.2.1 Simulation Results

In order to verify our estimate, we have incorporated a deep inelastic scattering Monte Carlo (LEPTO). As expected, most of the pions are produced at much larger angles compared to the Møller electrons. This is shown in Fig. 13. The acceptance Møller stripe is also shown for reference.

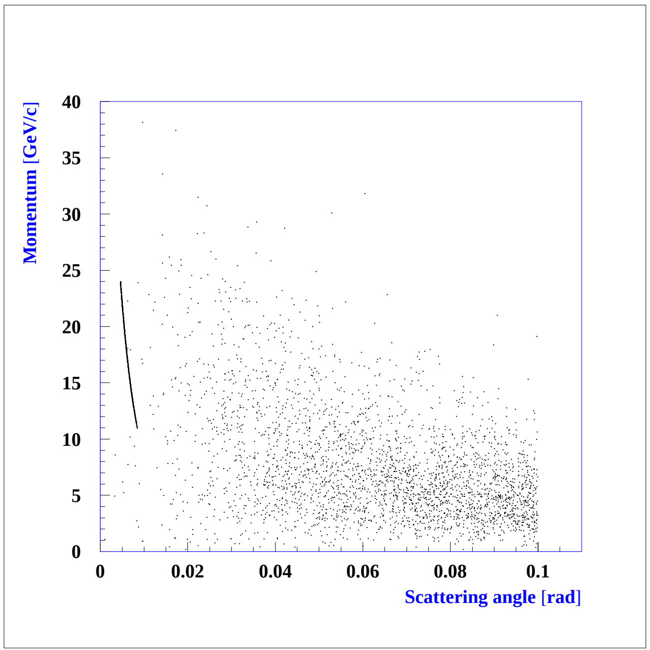

Figure 13: Scatter plot of the energy vs laboratory scattering angle of DIS pions is shown, along with the accepted Møller electron stripe.

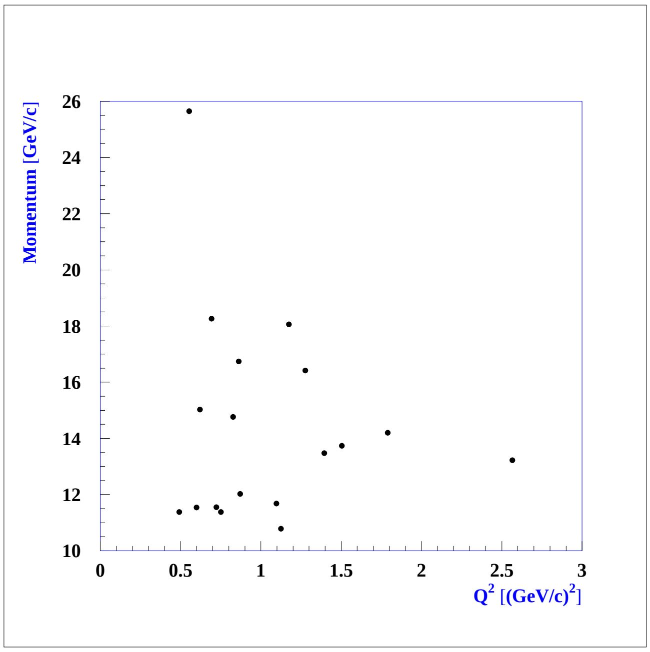

Figure 14: A scatter plot of the pion momentum vs the Q^2 of the scattered electron for events that arrive at the Møller detector are shown.

Figure 14 shows the pion momentum vs the Q^2 of the scattered electron (which determines the size of the electroweak asymmetry) for charged particles that arrive at the Møller detector. The luminosity corresponds to 500000 Møller electrons incident at the detector. It turns out that the majority of the particles are pions and a small fraction are muons and antiprotons. From this, we can conclude that the accepted rate from deep inelastic scattering leads to a dilution factor of less than 10^{-4} and the asymmetry correction is about 1%, agreeing with the calculation presented in Appendix C.5 of the proposal.

6.2.2 Integrating Pion Detector

Since the pions from deep inelastic scattering are a very small fraction of the signal, it will be hard to verify the actual rates or the Q^2 distribution of pions that are measured at the Møller detectors. We are therefore planning to monitor the asymmetry behind the Møller detector and 1 to 2 interaction lengths of absorber (see Fig. 2), where the rate should be dominated by punchthrough pions. Using the rate of accepted pions from the Monte Carlo simulation, we estimate that we would measure an electroweak asymmetry of between 50 and 100 ppm with a statistical accuracy better than 10%.

7 Summary

We summarize our main results on the spectrometer design, backgrounds and comment on the plan for commissioning in the following sections.

7.1 Spectrometer Design

We itemize important progress in the design of the spectrometer since the proposal below:

- We have evolved the design of the dipole chicane (different first dipole, slightly different positioning) in order to incorporate better shielding while ensuring no loss of acceptance.
- We have designed optimal collimators to shield the detectors from photons without any significant loss of acceptance or degradation of backgrounds.
- We have incorporated two special collimators to shield the detectors from synchrotron radiation from the dipole chicane with less than 5% acceptance loss.
- We have studied energy deposition in ESA and pinpointed the regions of the spectrometer that require cooling.
- We have incorporated new counting detectors that will allow us to study electron kinematics in detail and verify the optics of the spectrometer.
- We have carried out new studies of Mott and pion backgrounds and firmed up the calculations presented in the proposal.

7.2 Backgrounds

We summarize and update the table of backgrounds presented in the original proposal in Table 2.

Our main conclusions are:

- Pions are a negligible component ($< 1\%$) of the total rate into the Møller detectors.
- The DIS pion asymmetry will be measured quite accurately by the pion integrating detector.
- The counting detectors will be very important in evaluating the systematic errors in the background subtraction.
- Additional work on radiative inelastic resonance electroproduction would be useful.
- Monte Carlo work can now begin to optimize the design of the counting detectors.

Process	σ/σ_M	δA
elastic $e-p$	0.15	0.07
Inelastic $e-p$	2×10^{-3}	0.02
Δ Electroproduction	2.5×10^{-3}	0.01
Resonance Electroproduction	3.0×10^{-3}	0.01
Other Electroproduction	2.0×10^{-3}	0.01
πs from DIS	$1.3{\times}10^{-5}$	0.01
πs from $\gamma(^*) - P$	$1.5{\times}10^{-4}$	0.002

Table 2: Summary Table of Physics Background Estimates

7.3 Commissioning Plans

A chart of the schedule for ESA commissioning is shown in Fig. 15. Our goal is to be ready for physics in late 2000 (beginning of fiscal 2001). The cleanup of ESA will begin immediately after the completion of E155X. The downstream end of ESA will begin commissioning in late Fall. In Spring '00, all magnetic elements, collimators and the beam pipes will be installed.

We are focusing the E158 commissioning efforts around two run periods, for which we plan to make requests:

1. An electron source asymmetry control commissioning run at 1 GeV to the ASSET region in late 99 - early 00.

2. A spectrometer commissioning run in summer at 48 GeV in summer 00.

Successful commissioning runs will ensure that we will be ready as planned for a physics run in fiscal 01.

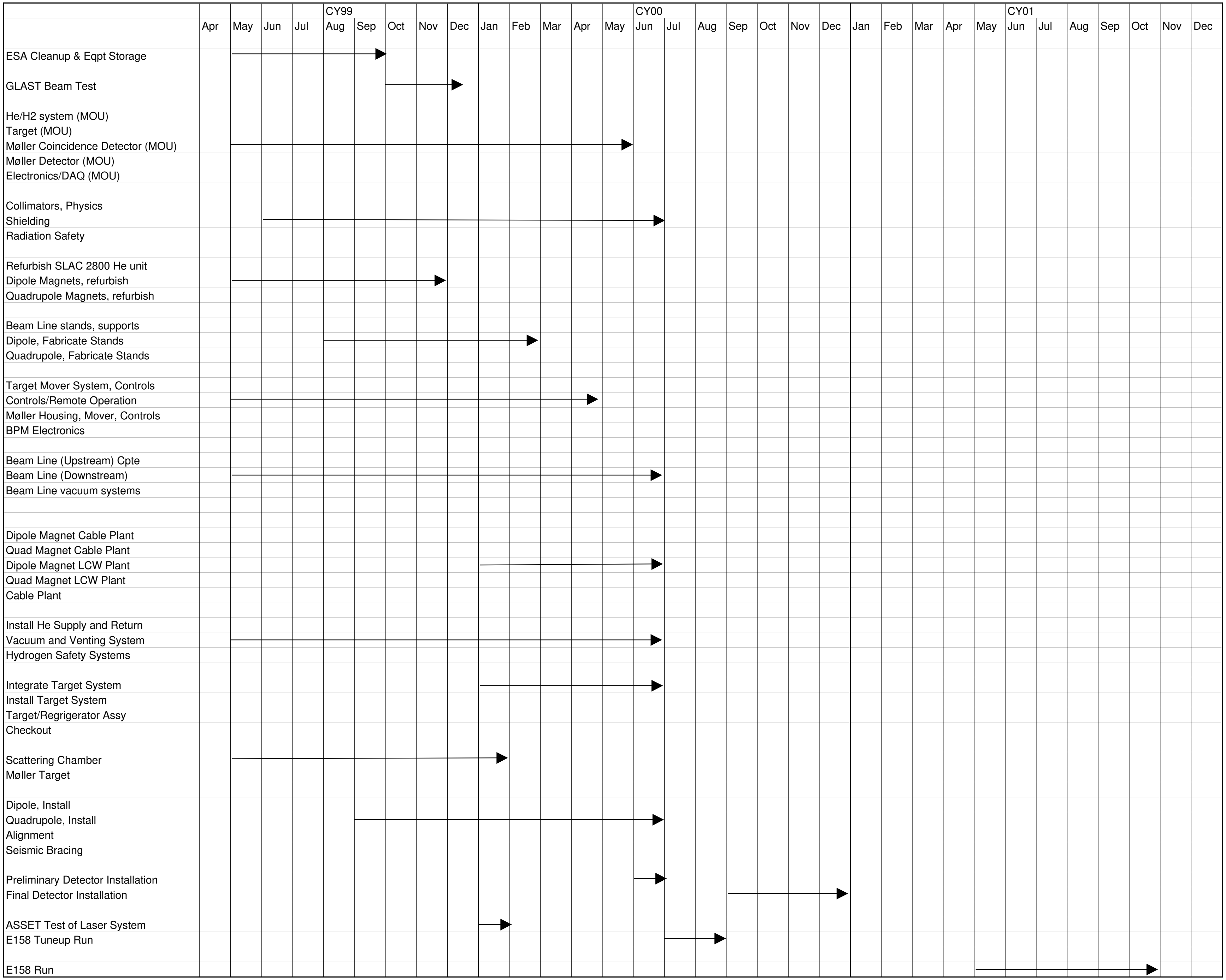

Figure 15: E158 ESA commissioning plan